Mitotic chromatin marking governs asymmetric segregation of DNA damage

Juliette Ferrand[1], Juliette Dabin[1], Odile Chevallier[1], Ariana Kupai[2], Scott B. Rothbart[2], Sophie E. Polo[1]†

[1] Laboratory of Epigenome Integrity, Epigenetics & Cell Fate Centre, UMR7216 CNRS, Université Paris Cité, Paris, France
[2] Department of Epigenetics, Van Andel Institute, Grand Rapids, MI, USA.

†Corresponding author. Email: sophie.polo@univ-paris-diderot.fr (S.E.P)

SUMMARY

The faithful segregation of intact genetic material and the perpetuation of chromatin states through mitotic cell divisions are pivotal for maintaining cell function and identity across cell generations. However, most exogenous mutagens generate long-lasting DNA lesions that are segregated during mitosis. How this segregation is controlled is unknown. Here, we uncover a mitotic chromatin-marking pathway that governs the segregation of UV-induced damage in human cells. Our mechanistic analyses reveal two layers of control: histone ADP-ribosylation, and the incorporation of newly synthesized histones at UV damage sites, that both prevent local mitotic phosphorylations on histone H3 serines. Functionally, this chromatin-marking pathway drives the asymmetric segregation of UV damage in the cell progeny with potential consequences on daughter cell fate. We propose that this mechanism may help preserve the integrity of stem cell compartments during asymmetric cell divisions.

INTRODUCTION

Genome integrity is constantly challenged by external and internal sources of genotoxic stress [1,2]. Cells have evolved elaborate pathways to repair DNA damage and to monitor genome integrity at critical steps of the cell cycle, thus preventing the transmission of damaged material across cell divisions [3–5]. Nevertheless, some DNA lesions escape classical checkpoint control and are transmitted to the cell progeny, sometimes unevenly, with adverse consequences on daughter cells inheriting the damage [6]. In particular, long-lasting DNA damage generated by exogenous mutagens such as UV light persist through mitosis, and their non-random segregation through multiple cell generations shapes cancer genome evolution [7]. Replication-associated endogenous damage, including under-replicated DNA, can also be passed on to the next cell cycle to be resolved in daughter cells [6,8,9]. Non-random segregation of replicative damage is dependent on the ATR-Chk1 kinase pathway [6,10]. However, control mechanisms for

exogenous DNA damage segregation during cell division are unknown. The DNA damage response is accompanied by a reshaping of the chromatin landscape, including critical changes in histone post-translational modifications (PTMs) [11]. It is thus tempting to speculate that alterations in histone PTMs closely associated with mitotic events [12] may contribute to control the segregation of DNA damage during cell division. Supporting this hypothesis, the mitotic histone mark threonine 3 phosphorylation on histone H3 (H3T3ph) drives asymmetric segregation of chromatin during the division of Drosophila male germline stem cells [13]. We thus decided to examine H3 mitotic phosphorylations during the response of human cells to UV-induced damage and their potential consequences on DNA damage segregation.

RESULTS

Non-random segregation of UV-damaged chromosomes through mitosis

Cells locally damaged with UV still divide and transmit the damaged material to the progeny, resulting in an easily identifiable scattered pattern of DNA damage in daughter cells (Figure 1A, red dots in G1 cell nuclei). To evaluate if post-replicative UV lesions are transmitted symmetrically or asymmetrically between daughter cells, we inflicted local UVC irradiation to cells synchronized at the G2/M boundary (Figure S1A) and measured the levels of the main UV photoproducts, CPDs (Cyclobutane Pyrimidine Dimers), in early G1 cells (Figure 1A). Of note, CPD signals show a linear correlation with the UV dose and thus are reliable measurements of UV-induced DNA damage (Figure S1B). We calculated the CPD bias in daughter cell pairs, which reflects the degree of asymmetry in UV damage distribution between daughter cells. We observed a wide range of UV damage segregation modes, from almost completely symmetric (ca. 1% CPD bias), meaning that daughter cells inherit similar amounts of DNA damage, to very asymmetric (ca. 60% CPD bias), where most of the DNA damage ends up in one daughter cell (Figure 1A). CPD repair was negligible during the first hours

following UV irradiation (Figure S1C), indicating that the observed CPD bias was not due to differential repair of UV lesions in daughter cells but was a bona fide DNA damage segregation bias. Remarkably, this segregation bias was observed both in cancer (U2OS, Figure 1A) and non-cancer cells (RPE-1, Figure S1D) with a 15% CPD bias on average in both cell types. This segregation bias is thus independent of cell aneuploidy and it does not reflect a general segregation defect of the genetic material since the damage segregation bias did not correlate with the total DNA segregation bias as measured by DAPI staining (Figure S1E). The UV damage segregation bias observed in G1 entails an asymmetrical distribution of UV lesions on sister chromatids. To further dissect this process, we analyzed the distribution of CPDs between sister chromatids in metaphase, which showed close to 10% asymmetry (Figure 1B). We next calculated the CPD bias that would result from a random distribution of damaged sister chromatids between the two daughter cells and the maximum segregation bias that we would expect if the most damaged sister chromatids were transmitted to the same daughter cell (Figure 1C). Interestingly, the observed CPD bias in G1 cells is comparable to the maximum CPD bias and significantly higher than the bias resulting from random DNA damage segregation (Figure 1C). Together, these results demonstrate that UV-damaged material is segregated through mitosis in a non-random manner.

Local defect in H3 mitotic phosphorylations at UV damage sites

To dissect the chromatin-based mechanisms that control the non-random segregation of UV-induced damage during mitotic cell division, we chose to focus on mitotic histone PTMs. One of the most prominent histone PTM induced upon mitotic entry is phosphorylation on serine 10 of histone H3 (H3S10ph) [14,15]. We thus monitored the distribution of this mitotic phosphorylation by immunofluorescence in human cells locally irradiated with UV in late G2 and released at the G2/M boundary as above (Figure S1A). We observed a local defect in

mitotic H3S10ph at UV sites 1h after UVC irradiation in U2OS, primary BJ and RPE-1 cells (Figure 2A, Figures S2A-S2C) that correlated with the UV dose (Figure S2D). Mitotic phosphorylation on serine 28 of histone H3 (H3S28ph) showed a similar defect (Figure 2A). The reduction in H3S10ph and H3S28ph signals did not result from a local decompaction of chromatin since there was no significant decrease in total H3 density at UV sites, as measured for two different H3 variants (Figure 2A and Figure S2E). We next examined the kinetics of the H3 phosphorylation defect by irradiating cells at different time points before mitotic entry. These experiments revealed an early and transient defect of H3S10ph in UV-damaged chromatin, restricted to cells that experienced damage within 2 h before mitosis (Figure S2F). Importantly, the local defect in H3 mitotic phosphorylation at UV damage sites was not explained by the mislocalization or impaired activation of the corresponding kinase Aurora B [16], whose binding to chromatin (detergent-resistant fraction, Figure 2B and Figure S2G) and autophosphorylation on threonine 232 (Figure 2C and Figure S2H) were not significantly inhibited following UV irradiation. These findings uncover a local impairment of mitotic H3 phosphorylations in UV-damaged chromatin that is not due to a defect in the corresponding kinase activity, suggesting that the histone substrate may be unsuitable for the reaction.

UV-induced chromatin dynamics counteract H3S10ph deposition in UV-damaged chromatin

To characterize histone H3 features impeding its mitotic phosphorylation at UV damage sites, we first explored a potential interference with other H3 PTMs. The detection of neighboring methylation on lysine 9 of histone H3 (H3K9me), after treating fixed cells with lambda-phosphatase to circumvent H3K9 epitope masking by H3S10ph [17] (Figure S3A), revealed that H3K9me levels remained essentially unaffected at UV sites in early mitotic nuclei, ruling out their contribution to a local inhibition of H3S10ph in response to UV (Figure S3B). Instead,

taking advantage of a range of antibodies recognizing H3S10ph in the context of different H3K9me states (Figure S3C) [18], we noticed that the H3S10ph defect occurred preferentially on H3 devoid of H3K9 tri-methylation (H3K9me3) (detected by the CST and CMA311 antibodies, Figure S3D). This behavior is reminiscent of another H3S10 PTM, the DNA damage-induced ADP-ribosylation (ADPr), which is inhibited by neighboring H3K9me3 and antagonizes H3S10ph [19–21], hinting towards a possible crosstalk between H3S10 phosphorylation and ADPr by PARP1/2 enzymes (poly(ADP-ribose) polymerases) and their cofactor HPF1 (histone PARylation factor 1) (Figure 3A). Consistent with this hypothesis and previous reports [22,23], ADPr was enriched at UV damage sites (Figure S4A). Furthermore, histones represented the major substrates for mono-ADPr following UV irradiation (Figure S4B). Inhibition (Figure 3B) or knock-down (Figure S4C) of PARP enzymes abrogated the H3S10ph defect in cells damaged just before mitosis, revealing an early inhibitory effect of ADPr on H3S10ph at UV sites. Similarly, knocking-down the PARP cofactor HPF1, that regulates histone ADP-ribosylation in response to DNA damage [24], reduced H3S10ph defect at UV sites (Figure S4D), indicating that PARP and HPF1 act in concert to inhibit H3S10ph deposition in UV-damaged chromatin. Reciprocally, maintaining ADPr by inhibiting Poly(ADP-ribose) glycohydrolase (PARG) or by depleting ADP ribosylhydrolase 3 (ARH3), which specifically targets serine residues [19,25], led to a prolonged H3S10ph defect at UV sites, detectable in cells irradiated 3h before mitosis (Figure 3C and Figure S4E). To directly and unambiguously address the crosstalk between ADPr and phosphorylation on the H3S10 residue, we introduced in U2OS cells non-ADPribosylatable forms of SNAP-tagged H3.1 or H3.3 by mutating S10 to a threonine (Figure S4F). Importantly, H3T10 can still be phosphorylated in early mitosis, as detected with an antibody that recognizes phosphorylation on both H3S10 and H3T10[26]. While a decrease in H3S10ph in response to UV irradiation was observed on endogenous histone H3 and on wild-type SNAP-tagged histones, as expected, the signal was unchanged on non-ADPribosylatable

histone mutants (Figure 3D), indicating that UV damage-induced ADPr on H3S10 blocks the phosphorylation of this residue in early mitotic chromatin. Together, our findings uncover a unique interference mechanism in UV-damaged chromatin where histone ADPr counteracts the deposition of a key mitotic phosphorylation mark on histone H3 at the G2/M transition.

New H3 deposition at UV sites delays mitotic H3S10ph

As the effect of histone ADPr on H3S10ph was restricted to cells damaged just before mitosis (observed 15 min before, Figure 3B, and not 1h before, Figure S5A), we searched for additional mechanisms that could contribute to the H3S10ph defect after the hydrolysis of ADPr chains. Newly synthesized H3 is incorporated at sites of UV damage repair [27,28] and displays less phosphorylation on S10 in early mitosis compared to old histones [29]. Newly synthesized H3 may thus be a poor substrate for mitotic phosphorylation, delaying H3S10ph deposition at UV sites. Interfering with new H3 deposition pathways by treating cells with siRNAs against H3.3 and the H3.1-specific chaperone CAF-1 (Chromatin Assembly Factor-1) blocked new H3 incorporation at UV sites (Figure 3E) and abolished the local defect in H3S10ph at UV sites in early mitotic cells (Figure 3F). In contrast, single depletions of H3.3, the H3.3 chaperone HIRA (Histone Regulator A), or the H3.1 chaperone CAF-1 had only a moderate effect on H3S10ph at UV sites (Figures S5B-D), indicating that *de novo* deposition of both H3 variants redundantly controls mitotic H3S10ph in UV-damaged chromatin. As an orthogonal approach, we interfered with new H3.1 and H3.3 deposition at UV sites by depleting the DNA damage sensor DDB2 (DNA damage binding protein 2) (Figure S5E), which also restored H3S10ph at UV damage sites (Figure S5F). This pathway appears to be distinct from the PARP-mediated mechanism described above since ADPr at UV sites was independent of DDB2 (Figure S5G). Thus, our findings reveal two independent layers of control, histone ADPr and new H3 deposition, both interfering with mitotic H3S10ph in UV-damaged chromatin.

The H3S10ph control pathway governs UV damage segregation in daughter cells

To test whether mitotic H3S10ph controls the DNA damage segregation process, we measured CPD levels in G1 daughter cells in two conditions showing opposite effects on H3S10ph at UV sites in early mitosis: UV irradiation 3h before mitosis, which does not lead to a detectable H3S10ph defect, vs. UV irradiation immediately before mitosis leading to an H3S10ph defect (Figure S2F). Remarkably, cells irradiated just before mitosis displayed a stronger bias of UV damage segregation between daughter cells in U2OS (Figure 4A). We obtained similar results in RPE-1 cells (Figure S6A) indicating that this phenomenon was not restricted to cancer cells. As the CPD signal remained unchanged throughout the experiment (Figure S1C), differences in segregation bias were not due to variable amounts of UV damage. Mechanistically, restoring H3S10ph by PARP inhibition significantly reduced the CPD segregation bias in daughter cells (Figure 4B and Figure S6B). Reciprocally, PARG inhibition, which prolongs the H3S10ph defect in early mitosis, resulted in an increased CPD segregation bias in G1 daughter cells (Figure 4B and Figure S6C). Note that PARP inhibition was applied to cells in late G2, thus avoiding the adverse mitotic consequences of PARP inhibition in S phase [30]. We attribute the result of PARP inhibition to the H3S10ph defect rather than to a distinct PARP-dependent process since the PARPi treatment on cells damaged 1h before mitotic entry did not interfere with H3S10ph deposition at UV sites (Figure S5A) and had no effect on DNA damage distribution between G1 cells (Figure S6D). Strengthening these findings, depletion of the DNA damage sensor DDB2, which also abrogates the H3S10ph defect, similarly reduced the UV damage segregation bias (Figure 4C). We conclude that the H3S10ph control pathway that marks damaged chromatin in early mitosis governs the asymmetric segregation of UV damage in daughter cells.

DISCUSSION

Understanding how chromatin integrity and cell identity are preserved from deleterious genotoxic stress through cell divisions is of fundamental importance. By studying mitotic phosphorylations on histone H3 in response to UV damage, our work sheds light on a chromatin-based mechanism that governs the non-random segregation of DNA lesions. We identify two complementary pathways that interfere with mitotic H3S10ph in UV-damaged chromatin, with an early contribution of histone ADP-ribosylation and a later contribution of newly deposited histone H3 (Figure 4D). Our findings support a model where the resulting H3S10ph defect may drive the asymmetric segregation of UV-damaged chromatin in daughter cells, with potential consequences on cell fate.

Our study also provides important insights into the so far elusive roles of histone ADPr and new histone deposition at DNA damage sites. We demonstrate that they both contribute to bookmark damaged chromatin during a crucial stage of the cell cycle by interfering with H3 mitotic phosphorylation. This function of histone ADP-ribosylation is likely distinct from its recently reported role in promoting chromatin relaxation at DNA double-strand breaks in human cells [24]. We provide evidence for a direct interference between ADPr and phosphorylation on H3S10 and the same likely applies to H3S28 because those two residues are the main targets of damage-induced ADPr [21]. Notably, a similar interplay between H3S10/28 ADPr and phosphorylation was recently reported in response to DNA double-strand breaks in amoeba, impacting mitotic entry of cells with unresolved damage[26]. Regarding newly synthesized H3, we suspect that they impair H3S10ph because they may represent poor substrates for Aurora B due to their specific PTM pattern. Indeed, Aurora B preferentially phosphorylates S10 on hypoacetylated H3 tails [31], while new H3 is enriched for acetylation on lysines 14 and 23 [32]. We note that besides these effects at the level of the histone substrate, we cannot rule out a possible contribution of phosphatases in H3S10ph removal from UV-damaged

chromatin, as reported in G1 cells after ionizing radiation-induced damage [33]. We did not notice any negative impact of UV damage on the Aurora B kinase in contrast to the PARP-dependent inhibition of Aurora B reported following oxidative damage [34].

A major conclusion of our work is the characterization of non-random segregation of post-replicative UV damage in the cell progeny. We propose that the local alteration in mitotic H3 phosphorylation could drive the asymmetric segregation of DNA damage, thus impacting daughter cell fate. An analogy can be drawn with another mitotic phosphorylation on H3T3, which governs asymmetric segregation of histone proteins and daughter cell fates in the Drosophila male germline [13]. Similar to H3S10ph, H3T3ph distinguishes pre-existing from newly synthesized histones. H3T3ph drives the asymmetric segregation of old and new histones in daughter cells because old and new histones H3 are asymmetrically distributed on the two strands during replication in Drosophila [35,36], while in mammalian cells they distribute symmetrically [37]. We propose that the induction of post-replicative UV damage in human cells may generate a local asymmetry at the histone level between sister chromatids, allowing the asymmetric segregation of DNA damage in daughter cells. How the H3S10ph defect at UV sites is mechanistically connected to the asymmetric distribution of damaged chromosomes is a pending question. This may rely on an asymmetry in the chromosome segregation machinery with asymmetric microtubule assembly and attachment to kinetochores, as described in Drosophila [38,39]. A local lack of histone phosphorylation may also affect the electrostatic properties of mitotic chromatin, known to control chromosome separation [40,41], which would favor the co-segregation of damaged chromatids. We speculate that the damaged material would be preferentially inherited by differentiated cells, shown to repair UV damage more efficiently[42], thus preserving the stem cell compartment. This is particularly important in stem cells, which are devoid of classical cell cycle checkpoints, and would contribute to control genome stability at the tissue scale. An interesting possibility that deserves further investigation

is that the non-random segregation of UV damage may be accompanied by an asymmetric distribution of repair proteins, reflecting distinct repair capacities in daughter cells, as described following replication stress [6,10]. Given that we observed a UV damage segregation bias in U2OS and RPE-1 cells, which divide symmetrically, the non-random segregation of UV damage is more likely a cause than a consequence of distinct daughter cell fates. Supporting the hypothesis that the daughter cell inheriting more damage may adopt a differentiated fate, the DNA damage response is known to promote cell differentiation [43]. Studying the damage response in physiological models that harbor asymmetric cell divisions will be of high interest to address the functional consequences of non-random damage segregation on cell identity.

METHODS

Cell culture and drug treatments

BJ primary fibroblasts (ATCC CRL-2522, human foreskin, male), U2OS cells (ATCC HTB-96, human osteosarcoma, female) and RPE-1 hTERT cells (ATCC CRL-4000, human retinal pigment epithelium, female) were grown at 37°C and 5% CO_2 in Dulbecco's modified Eagle's medium (DMEM, Invitrogen) supplemented with fetal calf serum (EUROBIO, 15% final for BJ and 10% final for U2OS and RPE-1) and antibiotics (100 U/ml penicillin, 100 µg/ml streptomycin, Invitrogen). U2OS cells stably expressing H3.1-SNAP, H3.3-SNAP, and GFP-XPC were grown in the same medium supplemented with selection antibiotics (Supplementary Table 1). The PARP inhibitor KU-58948 (Axon MedChem) was added to the culture medium at 10 µM final concentration 1 h prior UV irradiation. Cells were treated overnight with the PARG inhibitor (Sigma-Aldrich) at 1 µM final concentration. Oxidative damage was induced by treating cells for 10 min with 2 mM hydrogen peroxide (H_2O_2, Sigma-Aldrich).

Stable cell lines	Selection antibiotics	References
U2OS H3.1-SNAP	100 µg/ml G418	44
U2OS H3.3-SNAP	100 µg/ml G418	44
U2OS H3.3-SNAP GFP-XPC	100 µg/ml G418 + 200 µg/ml Hygromycin	45

Supplementary Table 1. Stable cell lines. Antibiotics: Hygromycin, G418 (Euromedex).

Site directed mutagenesis

The mutation of Serine 10 to Threonine (S10T) was introduced by site directed mutagenesis on C-terminal SNAP-tagged H3.1 (HIST1H3C coding sequence cloned in pSNAPm) and H3.3 (H3F3B coding sequence cloned in pSNAPm) encoding plasmids with a PCR master kit (Roche) and the primers indicated in Supplementary table 2. U2OS cell lines stably expressing the mutated H3.1 or H3.3 S10T were generated by transfection of the plasmids with

Lipofectamine 2000 (Invitrogen). The clones were selected in medium supplemented with G418 (Life Technologies) starting 48h after transfection. Cells were grown in the same conditions as described above for U2OS cells expressing wild-type H3.1-SNAP or H3.3-SNAP. Clones were selected based on total levels of SNAP-tagged histones (see section SNAP labeling of histone proteins) compared to U2OS cells expressing wild-type H3.1-SNAP or H3.3-SNAP.

Mutated amino-acid	Histone gene	Mutated codon	Position in CDS	Mutagenesis primer sequence
S10T	H1ST1H3C	TCT → ACC	31 and 33	F: 5'-AGCTTTGCCGCCGGTGGTCTTGCGAGCTGTTTG-3' R: 5'-CAAACAGCTCGCAAGACCACCGGCGGCAAAGCT-3'
	H3F3B	TTC → ACC	31	F: 5'-CAGACTGCTCGTAAGACCACCGGTGGGAAAG-3' R: 5'-CTTTCCCACCGGTGGTCTTACGAGCAGTCTG - 3'

Supplementary Table 2. Primers for site directed mutagenesis. CDS: coding sequence; F: forward; R: reverse.

Cell synchronization

Cell cultures were enriched in early mitotic cells by overnight treatment with 2 mM Thymidine (Sigma-Aldrich), followed by a 6-8h release in fresh medium, and overnight treatment with 10 µM of the Cdk1 inhibitor RO-3306 (Merck Millipore). Cells arrested in late G2 were then allowed to enter mitosis with a 15-min release in fresh medium. To harvest cells in G1 instead of early mitosis, cells were released from the Cdk1 inhibitor for 1h30 in fresh medium.

UVC irradiation

Local UVC irradiation was performed on cells grown on glass coverslips (VWR) covered with a polycarbonate filter (5 µm pore size, Merck Millipore) and irradiated with UVC (254 nm) using a low-pressure mercury lamp (Vilber-Lourmat). The UVC dose (300 J/m^2 unless stated otherwise) was controlled using a VLX-3W dosimeter (Vilber-Lourmat). For global irradiation, cells in PBS (Phosphate Buffer Saline) were exposed to 10 J/m^2 UVC.

SNAP labeling of histone proteins

Total SNAP-tagged histones were labeled by incubating cells with 2 µM of the red-fluorescent reagent SNAP-cell TMR-star (New England Biolabs) for 15 min before cell fixation. For specific labeling of neo-synthesized histones, pre-existing SNAP-tagged histones were quenched during 30 min with 10 µM of the non-fluorescent reagent SNAP-cell Block (New England Biolabs), followed by a 30-min wash in fresh medium and a 2-h chase. New histones synthesized during the chase step were labeled by incubating cells with the red-fluorescent SNAP reagent as described above or with SNAP-cell Oregon green at 4 µM (15-min pulse), followed by 30 min incubation in fresh medium. Local UVC damage was inflicted just before the pulse.

siRNA transfection

siRNA purchased from Eurofins MWG Operon or Sigma-Aldrich (Supplementary Table 3) were transiently transfected into cells using Lipofectamine RNAiMax (Invitrogen) at a final concentration of 25-60 nM in the culture medium following manufacturer's instructions. Cells were harvested 48-72 h after siRNA transfections or 24 h for siH3.3 alone.

siRNA	Designation	Vendor
siARH3 #1	5' AGGCTCCTATGGCAATGGA 3'	Sigma-Aldrich
siARH3 #2	5' GAAGATTGGAGAGCTTCTA 3'	Sigma-Aldrich
siAuroraB	5′CAGAAGAGCTGCACATTTG 3′	Eurofins MWG Operon
siCAF-1 p60	5'AATCTTGCTCGTCATACCA 3'	Eurofins MWG Operon
siDDB2	5' TCACTGGGCTGAAGTTTAA 3'	Eurofins MWG Operon
siLUC	5' CGTACGCGGAATACTTCGA 3'	Eurofins MWG Operon
siH3.3	1 :1 combination of siH3.3A : 5' CTACAAAAGCCGCTCGCAA 3' and siH3.3B : 5' GCTAAGAGAGTCACCATCAT 3'	Eurofins MWG Operon
siHIRA	5' GAAGGACTCTCGTCTCATG 3'	Eurofins MWG Operon
siHPF1 #1	5' CTTCGAAAAGAAGTAGAAA 3'	Sigma-Aldrich
siHPF1 #2	5' CAGTAGATAAAAATGATGT 3'	Sigma-Aldrich
siHPF1 #3	5' CCAGTGACCTTCGAAAAGATT 3'	Sigma-Aldrich
siPARP1	5' GGGCAAGCACAGTGTCAAA 3'	Eurofins MWG Operon
siPARP2	5' AGATGATGCCCAGAGGAAC 3'	Eurofins MWG Operon

Supplementary Table 3. siRNA sequences

Immunofluorescence

Cells grown on glass coverslips (VWR) were fixed with 2% paraformaldehyde for 15 min and then permeabilized in 0.2% Triton-X-100 in PBS. For SNAP labeling experiments on asynchronous cell populations and for the detection of chromatin-bound Aurora B, cells were subject to detergent-permeabilization with 0.5% Triton-X-100 in CSK buffer (Cytoskeletal buffer: 10 mM PIPES pH 7.0, 100 mM NaCl, 300 mM Sucrose, 3 mM $MgCl_2$) for 5 min before fixation (pre-extraction). When performed on G2/M synchronized samples, pre-extraction conditions were milder with 0.1% Triton-X-100 in CSK buffer for 1 min to preserve early mitotic cells. For CPD staining, samples were denatured with 0.5 M NaOH for 5 min after fixation. To reveal H3K9 epitopes in early mitotic nuclei, cells were treated after fixation with λ-phosphatase (400 units final, New England Biolabs) for 30 min at 37°C as indicated in the manufacturer's instructions [17]. After fixation and permeabilization, samples were blocked in 5% BSA (Bovine Serum Albumin, Sigma-Aldrich) in PBS supplemented with 0.1% Tween 20 (Euromedex) and then incubated sequentially with primary antibodies and secondary antibodies conjugated with Alexa Fluor dyes (Supplementary Table 4). Coverlips were mounted in Vectashield or Vectashield plus antifade medium with DAPI (Vector Laboratories).

Type	**Antibody**	**Species**	**Dilution**	**Application**	**Supplier/ lab source**
Primary	ARH3	Rabbit	1:1000	WB	Sigma-Aldrich (HPA027141)
	Aurora B	Rabbit	1:500	IF	Sigma-Aldrich (SAB5600088)
	CAF-1 p60	Rabbit	1:10000	WB	Abcam (ab109442)
	CPD	Mouse	1:1000	IF	Kamiya Biomedical Company (MC-062)
	Cyclin B1	Mouse	1:250	IF	Santa Cruz Biotechnology (sc-245)
	DDB2	Mouse	1:200	WB	Abcam (ab51017)

	H3	Rabbit	1:10000 to 1:20000	WB	Abcam (ab1791)
	H3.3	Rabbit	1:1000	WB	Merck Millipore (09-838)
	H3K9me1	Rabbit	1:50	IF	Abcam (ab9045)
	H3K9me2	Rabbit	1:250	IF	Diagenode (C15410060)
	H3K9me3	Rabbit	1:500	IF	Abcam (ab8898)
	H3S10ph	Mouse	1:1000	IF	Cell Signaling (9706)
	H3S10ph	Rabbit	1:1000	IF, WB	Genetex (GTX128116)
	H3S10ph	Rat	1:1000	IF	Active Motif (61623)
	H3S10ph	Rabbit	1:50-1:1000	WB	Life Technologies (A301-844A-T)
	H3S10ph Fab CMA311	Mouse	1:1000	IF	Gift from H. Kimura's lab [18]
	H3S10ph Fab CMA 313	Mouse	1:1000	IF	Gift from H. Kimura's lab [18]
	H3S28ph	Rat	1:1000	IF	Sigma-Aldrich (H9908)
	HIRA	Mouse	1:200	WB	Active Motif (39557)
	HPF1	Rabbit	1:2000	WB	Novus Biologicals (NBP1-93973)
	Mono-ADPr	Rabbit	1:1000	WB	Gift from I. Matic's lab [21]
	PARP1	Rabbit	1:1000	WB	Cell Signaling Technology (9542)
	PARP2	Mouse	1:50	WB	Enzo Life Sciences (ALX-804-639-L001)
	Phospho Aurora A/B /C	Rabbit	1:2000	WB	Cell Signaling Technology (2914)
	Poly-ADPr	Rabbit	1:200	IF	Trevigen (4336-BPC-100)
	Tubulin	Mouse	1:10000	WB	Sigma-Aldrich (T9026)
	XPB	Rabbit	1:500	IF	Sigma-Aldrich (X0879)

	Anti-Mouse HRP	Goat	1:10000	WB	Jackson Immunoresearch (115-035-068)
Secondary	Anti-Rabbit HRP	Donkey	1:10000	WB	Jackson Immunoresearch (711-035-152)
	Anti-Mouse Alexa Fluor 488	Goat	1:1000	IF	Invitrogen (A11029)
	Anti-Rabbit Alexa Fluor 488	Goat	1:1000	IF	Invitrogen (A11034)
	Anti-Rat Alexa Fluor 488	Goat	1:1000	IF	Invitrogen (A11006)
	Anti-Rabbit Alexa Fluor 568	Goat	1:1000	IF	Invitrogen (A11036)
	Anti-Mouse Alexa Fluor 568	Goat	1:1000	IF	Invitrogen (A11031)
	Anti-Rabbit Alexa Fluor 594	Goat	1:1000	IF	Invitrogen (A11037)
	Anti-Mouse Alexa Fluor 594	Goat	1:1000	IF	Invitrogen (A11032)
	Anti-Rabbit Alexa Fluor 647	Goat	1:1000	IF	Invitrogen (A21245)
	Anti-Mouse Alexa Fluor 647	Goat	1:1000	IF	Invitrogen (A21236)

Supplementary Table 4: Antibodies. IF: Immunofluorescence; WB: Western-Blot

Specificity of H3S10ph antibodies

The specificities of H3S10ph antibodies used in this study (Supplementary Table 4) were tested on a histone peptide microarray as previously described [46]. Briefly, chemically synthesized C-terminally biotinylated histone H3 peptides bearing the modifications of interest were spotted onto streptavidin-coated slides using an Aushon 2470 microarrayer. Each peptide was printed

as 2 rows of 3 consecutive spots. Slides were hybridized with primary antibodies (CST 9706 1:1000, GTX 128116 1:2000, Abcam ab14955 1:1000) and Alexa Fluor 647-labeled secondary antibodies (Invitrogen A-21245, A-21235, A-21247, all at 1:5000 dilution). Hybridization steps were performed in buffer containing 25 mM HEPES pH 7.5, 100 mM NaCl, 0.5% BSA (w/v) and 0.1% NP-40 and washes in PBS supplemented with 0.1% Tween 20. Fluorescent signals were read on Innopsys InnoScan 1100AL microarray scanner and analyzed using ArrayNinja [47]. Values were normalized to the maximum signal on the array, and results are presented as mean values +/- SD from 6 spots/peptide.

Metaphase spreads

U2OS were synchronized in late G2 and damaged locally with the UVC lamp as described above prior to release in metaphase in medium containing 100 ng/ml Colcemid (Sigma-Aldrich) for 2h at 37°C. Cells were trypsinized, resuspended in a 75 mM KCl hypotonic solution for 15 min at 37°C and fixed with ethanol/acetic acid (v:v = 3:1) overnight at -20°C. The next day, the cells were dropped onto glass slides and air dried overnight. The cells on slides were fixed with 2% PFA and processed for immunostaining against the UV damage marker CPD (see Supplementary Table 4) as described above.

Cell extracts and western-blot

Total extracts were obtained by scraping cells in Laemmli buffer (50 mM Tris HCl pH 6.8, 1.6% Sodium Dodecyl Sulfate, 8% glycerol, 4% β-mercaptoethanol, 0.0025% bromophenol blue) followed by 5 min denaturation at 95°C. Total protein concentration was measured on a DS-11 FX+ spectrophotometer (DenoVix).

Extracts were run on 4-20% MINI-PROTEAN TGX gels (Bio-Rad) in running buffer (200 mM glycine, 25 mM Tris, 0.1% SDS) and transferred onto nitrocellulose membranes (Protran) with

a Trans-blot SD semidry transfer cell (Bio-Rad). Total proteins were revealed with Pierce reversible stain (Thermo Scientific). Proteins were probed with the appropriate primary antibodies and Horse Radish Peroxydase (HRP)-conjugated secondary antibodies (Supplementary Table 4). Protein detection by chemiluminescence was achieved using SuperSignal West Pico or Femto chemiluminescence substrates (Pierce) on hyperfilms MP (Amersham) processed in a SRX-101A tabletop film processor (Konica Minolta) or using the Odyssey Fc-imager (LI-COR Biosciences) following manufacturer's instructions. Quantification of protein levels was performed on images from the Odyssey Fc-imager with the Image Studio Lite software (version 5.2.5).

Flow cytometry

Cells were fixed in ice-cold 70% ethanol before DNA staining with 50 µg/ml Propidium Iodide (Sigma-Aldrich) in PBS containing 0.05% Tween 20 and 0.5 mg/ml RNaseA (USB/Affymetrix). DNA content was analyzed by flow cytometry (20,000 cells per condition) on a FACS Calibur Flow Cytometer (BD Biosciences) and data were processed with the FlowJo 9.7.5 software (Treestar) using both Watson and Dean/Jett/Fox algorithms for cell cycle analysis.

Image acquisition and analysis

Confocal images were captured on Zeiss LSM710/780/900 microscopes equipped with a Plan Apochromat 63x/1.4 and 40x/1.3 oil objective and Zen software. Epifluorescence imaging was performed on a Leica DMI6000 microscope using a Plan Apochromat 40x/1.3 or 63x/1.4 oil objective. Images were captured using a CCD camera (Photometrics) and Metamorph software. Images were assembled with Adobe Photoshop. Unprocessed images were analyzed with Image J software (U. S. National Institutes of Health, Bethesda, Maryland, USA,

http://imagej.nih.gov/ij/). Custom-made Image J macros were used for fluorescence quantifications in the damaged regions (defined by CPD signal or repair factor staining) and in the entire nucleus (delineated based on DAPI staining) after removal of background fluorescence signal. The enrichment/loss of proteins or histone marks at UV damage sites was given by the ratio of their mean intensities at UV sites relative to the whole nucleus. The UV damage segregation bias between daughter cells was calculated as the absolute difference of CPD intensities divided by the sum of CPD intensities measured in daughter cells. The resulting value was then converted into percent.

Statistical analysis

Statistical tests were performed using GraphPad Prism. Loss or enrichment of histone modifications or proteins of interest at UV sites relative to the whole nucleus was compared to a theoretical mean of 1 by one-sample t-test (two-sided). p-values for mean comparisons between two groups were calculated with a two-sided Student's t-test with Welch's correction. p-values for mean comparisons between more than two groups were calculated with a one-way ANOVA (Gaussian distribution and assuming equal SD). The Dunnett's correction was applied when samples were only compared with the control condition. Pearson correlation was applied to compare datasets. ns: non-significant, *: $p < 0.05$, **: $p < 0.01$, ***: $p < 0.001$, ****: $p < 0.0001$. Confidence interval of all statistical tests: 95%.

AUTHOR CONTRIBUTIONS

J.F. and J.D. designed and performed experiments with technical assistance from O.C., and analysed the data. J.F. and S.E.P. wrote the manuscript. A.K. and S.R. tested the antibodies with peptide arrays. S.E.P. supervised the project. All authors edited and approved the final version of the manuscript.

ACKNOWLEDGMENTS

We thank members of our laboratory for stimulating discussions and Slimane Ait-Si-Ali and Pierre-Antoine Defossez for critical reading of the manuscript. We thank H. Kimura and I. Matic for sharing antibodies. We acknowledge the help of the ImagoSeine facility (Institut Jacques Monod, France BioImaging) and of the imaging platform of the Epigenetics and Cell Fate Centre for confocal and epifluorescence microscopy. This work was supported by the European Research Council (starting grant ERC-2013-StG-336427 "EpIn" and consolidator grant ERC-2018-CoG-818625 "REMIND"), the French National Research Agency (ANR-18-CE12-0017-01 "HEROD"), the "Who am I?" laboratory of excellence (ANR-11-LABX-0071) funded by the French Government through its "Investments for the Future" program (ANR-11-IDEX-0005-01), and France-BioImaging (ANR-10-INBS-04). S.E.P. is an EMBO Young Investigator. J.F and J.D. received PhD fellowships from University Paris Diderot, Fondation ARC and EUR G.E.N.E (ANR-17-EURE-0013). S.B.R. acknowledges support from the National Institutes of Health (R35GM124736).

COMPETING INTERESTS STATEMENT

The authors declare no competing interests.

REFERENCES

1. Hoeijmakers, J.H.J. (2009). DNA Damage, Aging, and Cancer. New England Journal of Medicine *361*, 1475–1485. 10.1056/nejmra0804615.
2. Tubbs, A., and Nussenzweig, A. (2017). Endogenous DNA Damage as a Source of Genomic Instability in Cancer. Cell *168*, 644–656. 10.1016/j.cell.2017.01.002.
3. Branzei, D., and Foiani, M. (2010). Maintaining genome stability at the replication fork. Nat Rev Mol Cell Biol *11*, 208–219. 10.1038/nrm2852.
4. Ciccia, A., and Elledge, S.J. (2010). The DNA damage response: making it safe to play with knives. Mol Cell *40*, 179–204. 10.1016/j.molcel.2010.09.019.
5. Panagopoulos, A., and Altmeyer, M. (2021). The Hammer and the Dance of Cell Cycle Control. Trends Biochem Sci *46*, 301–314. 10.1016/j.tibs.2020.11.002.

6. Lezaja, A., Panagopoulos, A., Wen, Y., Carvalho, E., Imhof, R., and Altmeyer, M. (2021). RPA shields inherited DNA lesions for post-mitotic DNA synthesis. Nat Commun *12*, 3827. 10.1038/s41467-021-23806-5.
7. Aitken, S.J., Anderson, C.J., Connor, F., Pich, O., Sundaram, V., Feig, C., Rayner, T.F., Lukk, M., Aitken, S., Luft, J., et al. (2020). Pervasive lesion segregation shapes cancer genome evolution. Nature *583*, 265–270. 10.1038/s41586-020-2435-1.
8. Moreno, A., Carrington, J.T., Albergante, L., Al Mamun, M., Haagensen, E.J., Komseli, E.-S., Gorgoulis, V.G., Newman, T.J., and Blow, J.J. (2016). Unreplicated DNA remaining from unperturbed S phases passes through mitosis for resolution in daughter cells. Proceedings of the National Academy of Sciences *113*. 10.1073/pnas.1603252113.
9. Spies, J., Lukas, C., Somyajit, K., Rask, M.-B., Lukas, J., and Neelsen, K.J. (2019). 53BP1 nuclear bodies enforce replication timing at under-replicated DNA to limit heritable DNA damage. Nat Cell Biol *21*, 487–497. 10.1038/s41556-019-0293-6.
10. Xing, M., Zhang, F., Liao, H., Chen, S., Che, L., Wang, X., Bao, Z., Ji, F., Chen, G., Zhang, H., et al. (2020). Replication Stress Induces ATR/CHK1-Dependent Nonrandom Segregation of Damaged Chromosomes. Mol Cell *78*, 714-724.e5. 10.1016/j.molcel.2020.04.005.
11. Ferrand, J., Plessier, A., and Polo, S.E. (2021). Control of the chromatin response to DNA damage: Histone proteins pull the strings. Seminars in Cell & Developmental Biology *113*, 75–87. 10.1016/j.semcdb.2020.07.002.
12. Wang, F., and Higgins, J.M.G. (2013). Histone modifications and mitosis: countermarks, landmarks, and bookmarks. Trends Cell Biol *23*, 175–184. 10.1016/j.tcb.2012.11.005.
13. Xie, J., Wooten, M., Tran, V., Chen, B.-C., Pozmanter, C., Simbolon, C., Betzig, E., and Chen, X. (2015). Histone H3 Threonine Phosphorylation Regulates Asymmetric Histone Inheritance in the Drosophila Male Germline. Cell *163*, 920–933. 10.1016/j.cell.2015.10.002.
14. Hendzel, M.J., Wei, Y., Mancini, M.A., Van Hooser, A., Ranalli, T., Brinkley, B.R., Bazett-Jones, D.P., and Allis, C.D. (1997). Mitosis-specific phosphorylation of histone H3 initiates primarily within pericentromeric heterochromatin during G2 and spreads in an ordered fashion coincident with mitotic chromosome condensation. Chromosoma *106*, 348–360. 10.1007/s004120050256.
15. Goto, H., Kosako, H., Tomono, Y., Ajiro, K., Fujita, M., Sakurai, M., Okawa, K., Iwamatsu, A., Okigaki, T., Takahashi, T., et al. (1999). Identification of a Novel Phosphorylation Site on Histone H3 Coupled with Mitotic Chromosome Condensation. Journal of Biological Chemistry *274*, 25543–25549. 10.1074/jbc.274.36.25543.
16. Crosio, C., Fimia, G.M., Loury, R., Kimura, M., Okano, Y., Zhou, H., Sen, S., Allis, C.D., and Sassone-Corsi, P. (2002). Mitotic phosphorylation of histone H3: spatio-temporal regulation by mammalian Aurora kinases. Mol Cell Biol *22*, 874–885. 10.1128/MCB.22.3.874-885.2002.
17. Duan, Q., Chen, H., Costa, M., and Dai, W. (2008). Phosphorylation of H3S10 blocks the access of H3K9 by specific antibodies and histone methyltransferase. Implication in regulating chromatin dynamics and epigenetic inheritance during mitosis. J Biol Chem *283*, 33585–33590. 10.1074/jbc.M803312200.
18. Hayashi-Takanaka, Y., Yamagata, K., Nozaki, N., and Kimura, H. (2009). Visualizing histone modifications in living cells: spatiotemporal dynamics of H3 phosphorylation during interphase. J Cell Biol *187*, 781–790. 10.1083/jcb.200904137.
19. Fontana, P., Bonfiglio, J.J., Palazzo, L., Bartlett, E., Matic, I., and Ahel, I. (2017). Serine ADP-ribosylation reversal by the hydrolase ARH3. Elife *6*, e28533. 10.7554/eLife.28533.

20. Bartlett, E., Bonfiglio, J.J., Prokhorova, E., Colby, T., Zobel, F., Ahel, I., and Matic, I. (2018). Interplay of Histone Marks with Serine ADP-Ribosylation. Cell Rep *24*, 3488-3502.e5. 10.1016/j.celrep.2018.08.092.
21. Bonfiglio, J.J., Leidecker, O., Dauben, H., Longarini, E.J., Colby, T., San Segundo-Acosta, P., Perez, K.A., and Matic, I. (2020). An HPF1/PARP1-Based Chemical Biology Strategy for Exploring ADP-Ribosylation. Cell *183*, 1086-1102.e23. 10.1016/j.cell.2020.09.055.
22. Pines, A., Vrouwe, M.G., Marteijn, J.A., Typas, D., Luijsterburg, M.S., Cansoy, M., Hensbergen, P., Deelder, A., de Groot, A., Matsumoto, S., et al. (2012). PARP1 promotes nucleotide excision repair through DDB2 stabilization and recruitment of ALC1. J Cell Biol *199*, 235–249. 10.1083/jcb.201112132.
23. Robu, M., Shah, R.G., Purohit, N.K., Zhou, P., Naegeli, H., and Shah, G.M. (2017). Poly(ADP-ribose) polymerase 1 escorts XPC to UV-induced DNA lesions during nucleotide excision repair. Proc Natl Acad Sci U S A *114*, E6847–E6856. 10.1073/pnas.1706981114.
24. Smith, R., Zentout, S., Rother, M., Bigot, N., Chapuis, C., Mihuț, A., Zobel, F.F., Ahel, I., van Attikum, H., Timinszky, G., et al. (2023). HPF1-dependent histone ADP-ribosylation triggers chromatin relaxation to promote the recruitment of repair factors at sites of DNA damage. Nat Struct Mol Biol *30*, 678–691. 10.1038/s41594-023-00977-x.
25. Abplanalp, J., Leutert, M., Frugier, E., Nowak, K., Feurer, R., Kato, J., Kistemaker, H.V.A., Filippov, D. V, Moss, J., Caflisch, A., et al. (2017). Proteomic analyses identify ARH3 as a serine mono-ADP-ribosylhydrolase. Nat Commun *8*, 2055. 10.1038/s41467-017-02253-1.
26. Brustel, J., Muramoto, T., Fumimoto, K., Ellins, J., Pears, C.J., and Lakin, N.D. (2022). Linking DNA repair and cell cycle progression through serine ADP-ribosylation of histones. Nat Commun *13*, 185. 10.1038/s41467-021-27867-4.
27. Polo, S.E., Roche, D., and Almouzni, G. (2006). New Histone Incorporation Marks Sites of UV Repair in Human Cells. Cell *127*, 481–493. 10.1016/j.cell.2006.08.049.
28. Adam, S., Polo, S.E., and Almouzni, G. (2013). Transcription Recovery after DNA Damage Requires Chromatin Priming by the H3.3 Histone Chaperone HIRA. Cell *155*, 94–106. 10.1016/j.cell.2013.08.029.
29. Lin, S., Yuan, Z.-F., Han, Y., Marchione, D.M., and Garcia, B.A. (2016). Preferential Phosphorylation on Old Histones during Early Mitosis in Human Cells. J Biol Chem *291*, 15342–15357. 10.1074/jbc.M116.726067.
30. Slade, D. (2019). Mitotic functions of poly(ADP-ribose) polymerases. Biochem Pharmacol *167*, 33–43. 10.1016/j.bcp.2019.03.028.
31. Li, Y., Kao, G.D., Garcia, B.A., Shabanowitz, J., Hunt, D.F., Qin, J., Phelan, C., and Lazar, M.A. (2006). A novel histone deacetylase pathway regulates mitosis by modulating Aurora B kinase activity. Genes Dev *20*, 2566–2579. 10.1101/gad.1455006.
32. Alabert, C., Barth, T.K., Reverón-Gómez, N., Sidoli, S., Schmidt, A., Jensen, O.N., Imhof, A., and Groth, A. (2015). Two distinct modes for propagation of histone PTMs across the cell cycle. Genes Dev *29*, 585–590. 10.1101/gad.256354.114.
33. Sharma, A.K., Khan, S.A., Sharda, A., Reddy, D. V, and Gupta, S. (2015). MKP1 phosphatase mediates G1-specific dephosphorylation of H3Serine10P in response to DNA damage. Mutation Research/Fundamental and Molecular Mechanisms of Mutagenesis *778*, 71–79. 10.1016/j.mrfmmm.2015.06.001.
34. Monaco, L., Kolthur-Seetharam, U., Loury, R., Murcia, J.M., de Murcia, G., and Sassone-Corsi, P. (2005). Inhibition of Aurora-B kinase activity by poly(ADP-ribosyl)ation in response to DNA damage. Proc Natl Acad Sci U S A *102*, 14244–14248. 10.1073/pnas.0506252102.

35. Tran, V., Feng, L., and Chen, X. (2013). Asymmetric distribution of histones during Drosophila male germline stem cell asymmetric divisions. Chromosome Res *21*, 255–269. 10.1007/s10577-013-9356-x.
36. Wooten, M., Snedeker, J., Nizami, Z.F., Yang, X., Ranjan, R., Urban, E., Kim, J.M., Gall, J., Xiao, J., and Chen, X. (2019). Asymmetric histone inheritance via strand-specific incorporation and biased replication fork movement. Nat Struct Mol Biol *26*, 732–743. 10.1038/s41594-019-0269-z.
37. Petryk, N., Dalby, M., Wenger, A., Stromme, C.B., Strandsby, A., Andersson, R., and Groth, A. (2018). MCM2 promotes symmetric inheritance of modified histones during DNA replication. Science (1979) *361*, 1389–1392. 10.1126/science.aau0294.
38. Ranjan, R., Snedeker, J., and Chen, X. (2019). Asymmetric Centromeres Differentially Coordinate with Mitotic Machinery to Ensure Biased Sister Chromatid Segregation in Germline Stem Cells. Cell Stem Cell *25*, 666-681.e5. 10.1016/j.stem.2019.08.014.
39. Dattoli, A.A., Carty, B.L., Kochendoerfer, A.M., Morgan, C., Walshe, A.E., and Dunleavy, E.M. (2020). Asymmetric assembly of centromeres epigenetically regulates stem cell fate. J Cell Biol *219*, e201910084. 10.1083/jcb.201910084.
40. Cuylen, S., Blaukopf, C., Politi, A.Z., Müller-Reichert, T., Neumann, B., Poser, I., Ellenberg, J., Hyman, A.A., and Gerlich, D.W. (2016). Ki-67 acts as a biological surfactant to disperse mitotic chromosomes. Nature *535*, 308–312. 10.1038/nature18610.
41. Cuylen-Haering, S., Petrovic, M., Hernandez-Armendariz, A., Schneider, M.W.G., Samwer, M., Blaukopf, C., Holt, L.J., and Gerlich, D.W. (2020). Chromosome clustering by Ki-67 excludes cytoplasm during nuclear assembly. Nature *587*, 285–290. 10.1038/s41586-020-2672-3.
42. Li, W., Liu, W., Kakoki, A., Wang, R., Adebali, O., Jiang, Y., and Sancar, A. (2019). Nucleotide excision repair capacity increases during differentiation of human embryonic carcinoma cells into neurons and muscle cells. J Biol Chem *294*, 5914–5922. 10.1074/jbc.RA119.007861.
43. Sherman, M.H., Bassing, C.H., and Teitell, M.A. (2011). Regulation of cell differentiation by the DNA damage response. Trends Cell Biol *21*, 312–319. 10.1016/j.tcb.2011.01.004.
44. Dunleavy, E.M., Almouzni, G., and Karpen, G.H. (2011). H3.3 is deposited at centromeres in S phase as a placeholder for newly assembled CENP-A in G_1 phase. Nucleus *2*, 146–157. 10.4161/nucl.2.2.15211.
45. Adam, S., Dabin, J., Chevallier, O., Leroy, O., Baldeyron, C., Corpet, A., Lomonte, P., Renaud, O., Almouzni, G., and Polo, S.E. (2016). Real-Time Tracking of Parental Histones Reveals Their Contribution to Chromatin Integrity Following DNA Damage. Mol Cell *64*, 65–78. 10.1016/j.molcel.2016.08.019.
46. Cornett, E.M., Dickson, B.M., and Rothbart, S.B. (2017). Analysis of Histone Antibody Specificity with Peptide Microarrays. J Vis Exp, 55912. 10.3791/55912.
47. Dickson, B.M., Cornett, E.M., Ramjan, Z., and Rothbart, S.B. (2016). ArrayNinja: An Open Source Platform for Unified Planning and Analysis of Microarray Experiments. Methods Enzymol *574*, 53–77. 10.1016/bs.mie.2016.02.002.

FIGURE LEGENDS

Figure 1: Non-random segregation of UV damage through mitosis.

(A) Left: Experimental procedure for imaging UV damage segregation in G1 cells. Immunofluorescence images show an example of G1 daughter cells harboring scattered UV damage signal (CPD) reflecting the segregation of local UV damage inflicted before mitosis. Right: Pseudo-colored immunofluorescence images (lookup table shown on the right) of CPD distribution between G1 daughter cells (U2OS) to illustrate the symmetric versus asymmetric segregation of local UV damage inflicted before mitosis. The violin plot shows the CPD segregation bias in G1 daughter cells exposed to local UVC irradiation just before mitotic entry. (B) CPD distribution on sister chromatids analyzed by immunostaining on metaphase spreads from U2OS cells exposed to local UVC irradiation just before mitosis. A representative image is shown with a 2.5x zoom on a damaged chromosome. The CPD bias between each pair of sister chromatids from n damaged chromosomes is represented. (C) The expected CPD distribution bias in case of random chromatid segregation and the maximum bias in case of damage-driven chromatid segregation are compared to the observed CPD distribution bias in G1 daughter cells shown in panel (A). Violin plots show the mean of each independent experiment as a grey triangle ± SD from n cells (A, C) or damaged chromosomes (B). ****: $p < 0.0001$. Scale bars: 10 µm.

Figure 2: H3 phosphorylation defect at UV damage sites in early mitotic chromatin.

(A-B) H3 phosphorylation (H3S10ph, H3S28ph) and Aurora B kinase localization analyzed at the indicated times after local UVC irradiation in U2OS H3.3-SNAP cells synchronized in early mitosis. Damage sites are marked by XPB or CPD immunodetection and indicated by arrowheads. Dot plots show the mean of each independent experiment as a grey triangle ± SD

from n cells (colored dots). The significance of signal enrichment or loss at UV sites is indicated compared to a theoretical value of 1 (dotted line). ****: $p < 0.0001$. Fluorescence intensity profiles along the dotted lines are displayed on the graphs. (C) Levels of phosphorylated Aurora B (middle band, Thr232) and H3S10ph monitored by western-blot at the indicated time points post UVC irradiation in U2OS cells (Tubulin, loading control) with corresponding quantifications (mean ± SD from 4 independent experiments). The cell synchronization in G2/M was comparable in all conditions with around 20% of H3S10ph-positive cells scored by immunofluorescence. Scale bars: 10 µm.

Figure 3: Two independent mechanisms regulate H3S10ph deposition in UV-damaged chromatin.

(A) Working hypothesis for a potential crosstalk between phosphorylation and UV-induced ADP-ribosylation (ADPr) by the PARP-HPF1 axis on H3S10. The contributions of PARG and ARH3 to ADPr removal are indicated. (B-C) Immunostaining for H3S10ph at UV damage sites (marked by XPB or CPD) in early mitotic U2OS cells treated with the indicated inhibitors (PARPi; PARGi; -, vehicle) and harvested at the indicated times after local UVC irradiation. PARP and PARG inhibitor treatments are controlled by changes in the nuclear poly-ADPr signal measured by immunofluorescence (light blue dot plots). (D) Levels of H3S10ph monitored by western-blot 30 min post UVC irradiation in U2OS cell lines stably expressing wild-type (WT) or S10T mutated H3.1-SNAP or H3.3-SNAP in a wild-type H3 background (Tubulin, loading control). Quantification of H3S10ph on endogenous and SNAP-tagged H3 is shown on the graphs (mean ± SD from at least 3 independent experiments). (E) New histone H3.1 and H3.3 accumulation at UV damage sites analyzed after local UVC irradiation in asynchronous U2OS H3.1- or H3.3-SNAP cells treated with the indicated siRNAs (siLUC, control). New histones were labeled with SNAP-cell TMR star. (F) H3S10ph signal analyzed

by immunofluorescence after local UVC irradiation in U2OS H3.3-SNAP cells synchronized in early mitosis and treated with the indicated siRNAs (siLUC, control). UV damage sites are marked by XPB immunostaining. Knock-down efficiencies are controlled by western-blot (Tubulin, loading control). Dot plots show the mean of each independent experiment as a grey triangle ± SD from n cells (colored dots). Arrowheads point to UV-damaged regions. ****: $p < 0.0001$. Scale bars: 10 µm.

Figure 4: The UV-dependent H3S10ph control pathway biases DNA damage segregation in mitosis.

(A-C) Segregation of the DNA damage marker CPD assessed by immunostaining in G1 daughter cells (U2OS) treated with PARP or PARG inhibitors (B; -, vehicle) or depleted for the DNA damage sensor DDB2 (C; siLUC, control) and irradiated at the indicated time points before mitosis. Immunofluorescence images illustrate the corresponding H3S10ph pattern at UV sites (white arrowheads) in early mitosis for each condition. Knock-down efficiency is controlled by western-blot (Tubulin, loading control). Violin plots show the mean of each independent experiment as a grey triangle ± SD from n cells in total. ****: $p < 0.0001$. Scale bars: 10 µm. (D) Working model depicting the two layers of control that antagonize H3S10ph deposition at UV damage sites in early mitosis and their consequences on DNA damage segregation in daughter cells.

Figure 1

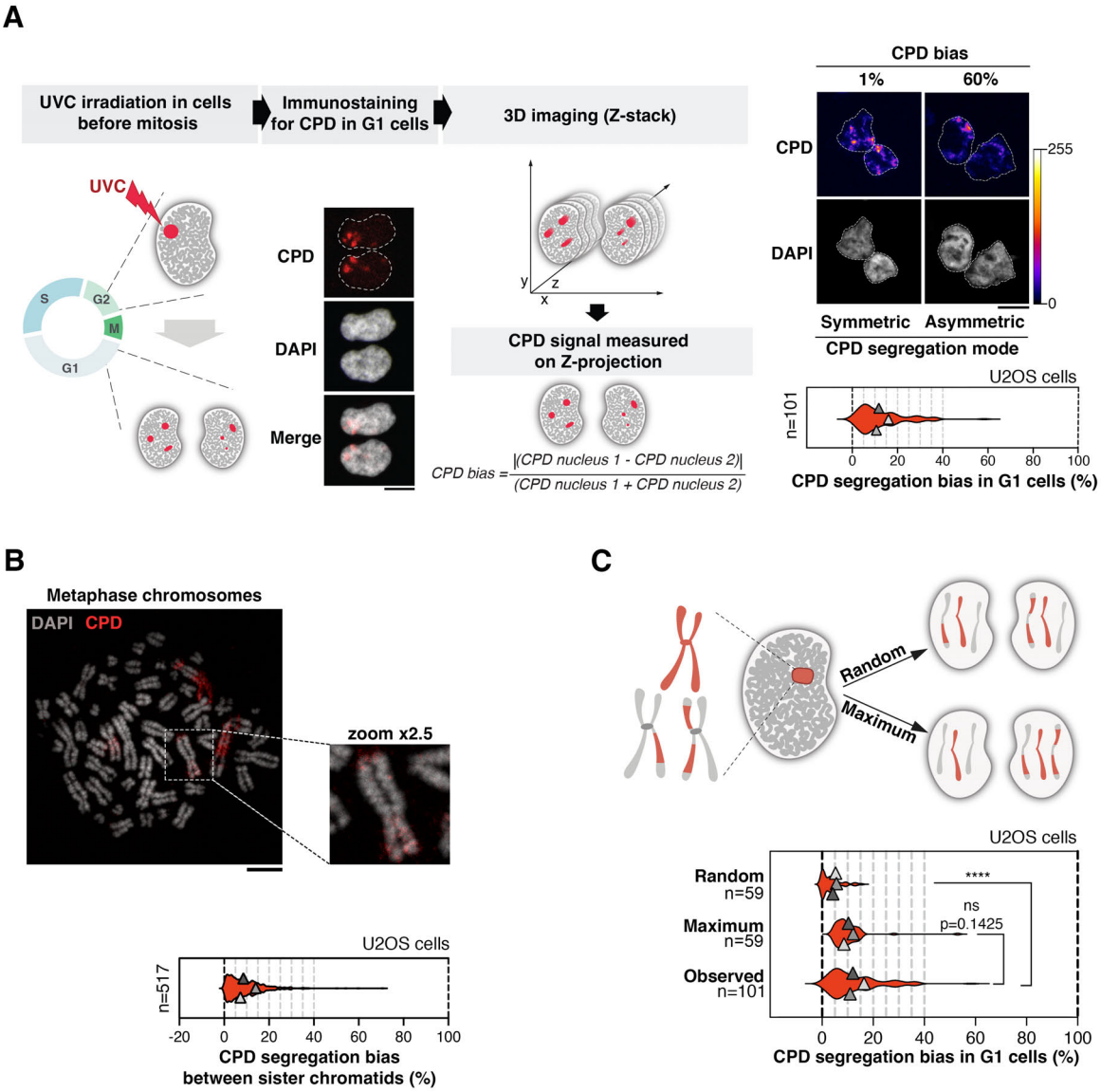
A
UVC irradiation in cells before mitosis
Immunostaining for CPD in G1 cells
3D imaging (Z-stack)
UVC
S
G2
M
G1
CPD
DAPI
Merge
y
z
x
CPD signal measured on Z-projection
CPD bias = |(CPD nucleus 1 - CPD nucleus 2)| / (CPD nucleus 1 + CPD nucleus 2)
CPD bias
1%
60%
CPD
DAPI
255
0
Symmetric
Asymmetric
CPD segregation mode
U2OS cells
n=101
0
20
40
60
80
100
CPD segregation bias in G1 cells (%)
B
Metaphase chromosomes
DAPI
CPD
zoom x2.5
U2OS cells
n=517
-20
0
20
40
60
80
100
CPD segregation bias between sister chromatids (%)
C
Random
Maximum
U2OS cells
Random
n=59
Maximum
n=59
Observed
n=101
****
ns
p=0.1425
0
20
40
60
80
100
CPD segregation bias in G1 cells (%)

Figure 2

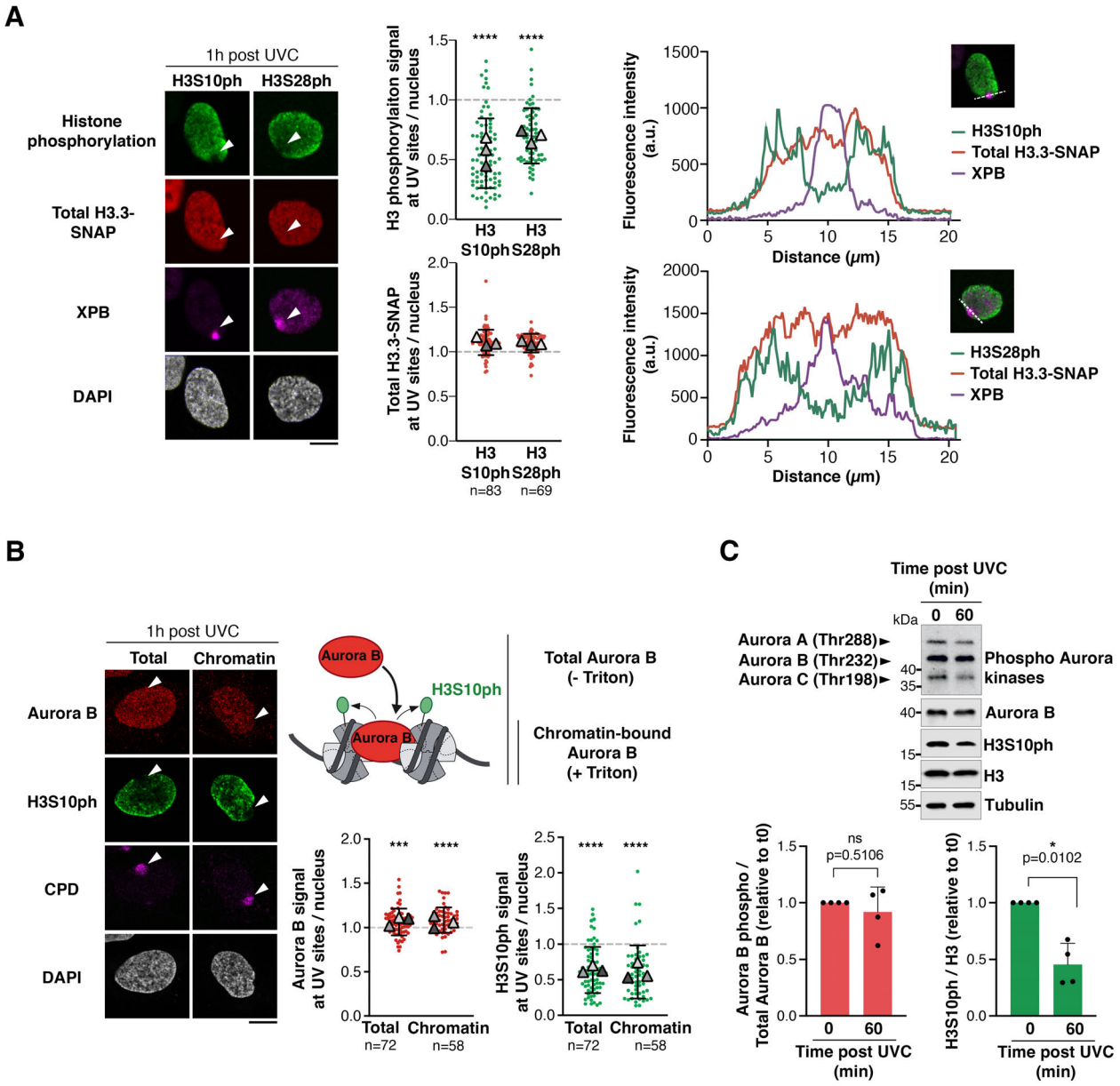
A
1h post UVC
H3S10ph
H3S28ph
Histone phosphorylation
Total H3.3-SNAP
XPB
DAPI
H3 phosphorylaiton signal at UV sites / nucleus
Total H3.3-SNAP at UV sites / nucleus
H3 S10ph
H3 S28ph
n=83
n=69
Fluorescence intensity (a.u.)
Distance (μm)
H3S10ph
Total H3.3-SNAP
XPB
H3S28ph
B
1h post UVC
Total
Chromatin
Aurora B
H3S10ph
CPD
DAPI
Aurora B
H3S10ph
Total Aurora B (- Triton)
Chromatin-bound Aurora B (+ Triton)
Aurora B signal at UV sites / nucleus
H3S10ph signal at UV sites / nucleus
Total
Chromatin
n=72
n=58
C
Time post UVC (min)
kDa
0
60
Aurora A (Thr288)
Aurora B (Thr232)
Aurora C (Thr198)
Phospho Aurora kinases
Aurora B
H3S10ph
H3
Tubulin
Aurora B phospho / Total Aurora B (relative to t0)
H3S10ph / H3 (relative to t0)
ns
p=0.5106
p=0.0102
Time post UVC (min)

Figure 3

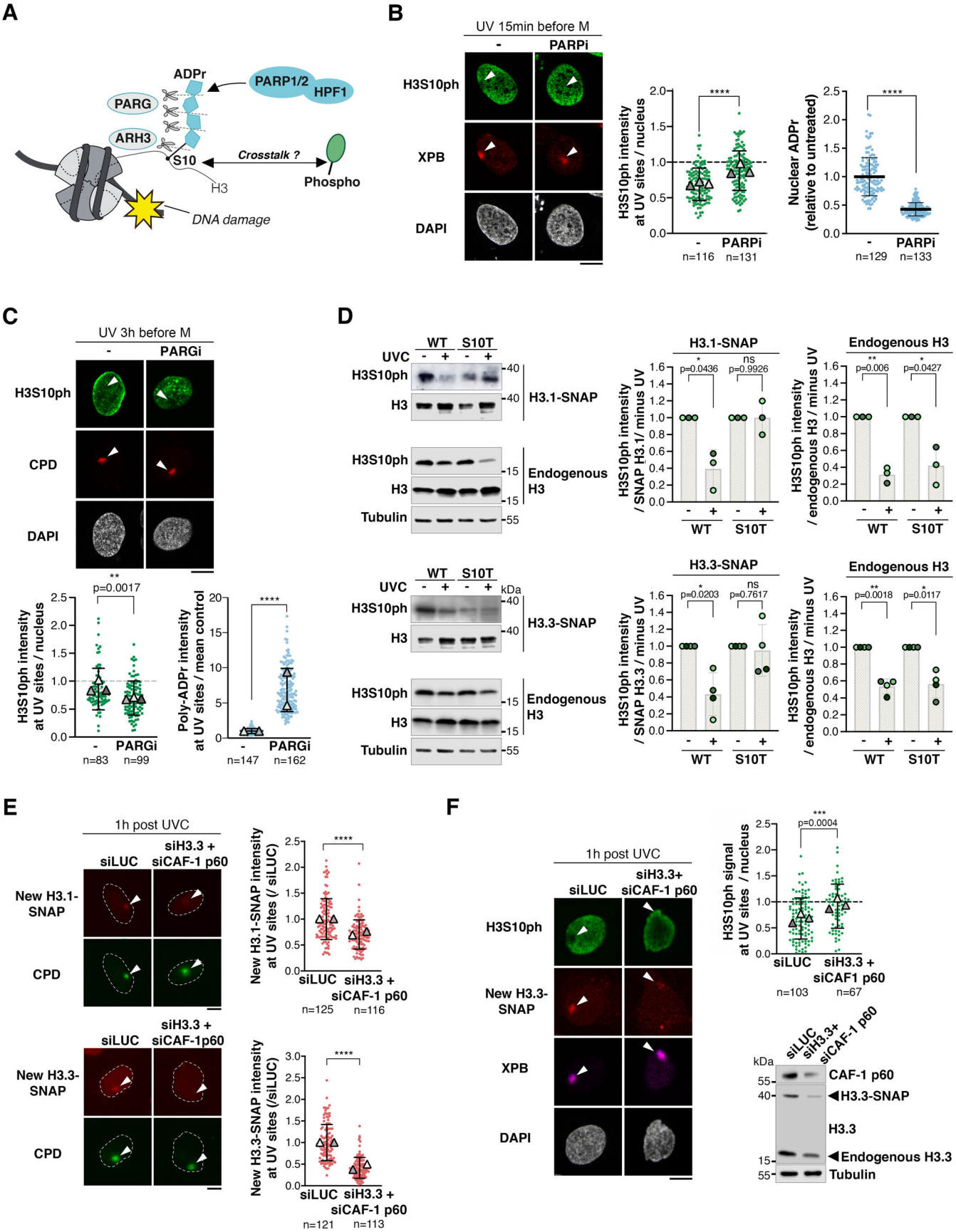
A
ADPr
PARP1/2
HPF1
PARG
ARH3
S10
Crosstalk ?
Phospho
H3
DNA damage
B
UV 15min before M
-
PARPi
H3S10ph
XPB
DAPI
H3S10ph intensity at UV sites / nucleus
****
n=116
n=131
Nuclear ADPr (relative to untreated)
n=129
n=133
C
UV 3h before M
PARGi
CPD
**
p=0.0017
n=83
n=99
Poly-ADPr intensity at UV sites / mean control
n=147
n=162
D
WT
S10T
UVC
kDa
H3.1-SNAP
Endogenous H3
Tubulin
H3.3-SNAP
H3.1-SNAP
H3.3-SNAP
Endogenous H3
p=0.0436
p=0.9926
p=0.006
p=0.0427
p=0.0203
p=0.7617
p=0.0018
p=0.0117
ns
E
1h post UVC
siLUC
siH3.3 + siCAF-1 p60
New H3.1-SNAP
New H3.3-SNAP
CPD
New H3.1-SNAP intensity at UV sites (/ siLUC)
New H3.3-SNAP intensity at UV sites (/siLUC)
n=125
n=116
n=121
n=113
F
siH3.3+ siCAF-1 p60
H3S10ph
XPB
DAPI
H3S10ph signal at UV sites / nucleus
***
p=0.0004
n=103
n=67
CAF-1 p60
H3.3-SNAP
H3.3
Endogenous H3.3
Tubulin

Figure 4

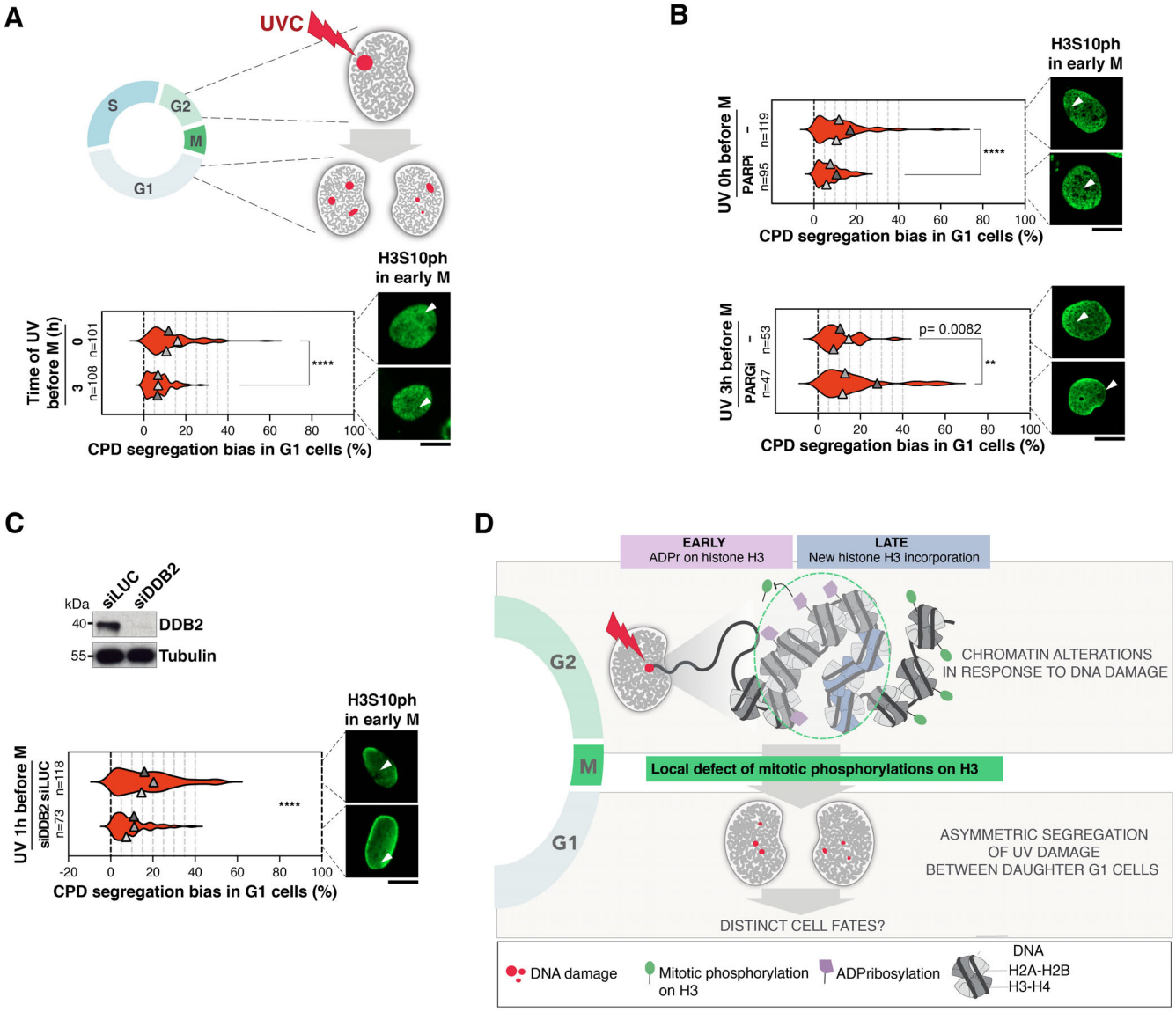
A
UVC
S
G2
M
G1
H3S10ph
in early M
Time of UV
before M (h)
0
n=101
3
n=108
****
0
20
40
60
80
100
CPD segregation bias in G1 cells (%)
B
H3S10ph
in early M
UV 0h before M
-
n=119
PARPi
n=95
****
CPD segregation bias in G1 cells (%)
UV 3h before M
-
n=53
PARGi
n=47
p= 0.0082
**
CPD segregation bias in G1 cells (%)
C
kDa
siLUC
siDDB2
40
DDB2
55
Tubulin
H3S10ph
in early M
UV 1h before M
siLUC
n=118
siDDB2
n=73
****
-20
0
20
40
60
80
100
CPD segregation bias in G1 cells (%)
D
EARLY
ADPr on histone H3
LATE
New histone H3 incorporation
G2
CHROMATIN ALTERATIONS
IN RESPONSE TO DNA DAMAGE
M
Local defect of mitotic phosphorylations on H3
G1
ASYMMETRIC SEGREGATION
OF UV DAMAGE
BETWEEN DAUGHTER G1 CELLS
DISTINCT CELL FATES?
DNA damage
Mitotic phosphorylation
on H3
ADPribosylation
DNA
H2A-H2B
H3-H4